International Journal of Nanomedicine

Dovepress
open access to scientific and medical research

Open Access Full Text Article

ORIGINAL RESEARCH

Synthesis of magnetic molecularly imprinted polymers with excellent biocompatibility for the selective separation and inhibition of testosterone in prostate cancer cells

This article was published in the following Dove Press journal:
International Journal of Nanomedicine
12 April 2017
Number of times this article has been viewed

Xiaoshuang Tang[1,2]
Feng Li[1]
Jing Jia[1]
Chao Yang[1]
Wei Liu[1]
Ben Jin[1]
Xinyang Wang[1]
Ruixia Gao[3]
Dalin He[1,4]
Peng Guo[1,4]

[1]Department of Urology, The First Affiliated Hospital of Xi'an Jiaotong University, [2]Department of Urology, The Second Affiliated Hospital of Xi'an Jiaotong University, [3]Institute of Analytical Science, School of Science, Xi'an Jiaotong University, [4]Key laboratory for Tumor Precision Medicine of Shaanxi Province, Xi'an, Shaanxi, People's Republic of China

Correspondence: Peng Guo
Department of Urology, The First Affiliated Hospital of Xi'an Jiaotong University, 277 Yan-Ta West Road, Xi'an, Shaanxi 710061, People's Republic of China
Tel +86 298 532 3661
Email guopeng661@mail.xjtu.edu.cn

Ruixia Gao
Institute of Analytical Science, School of Science, Xi'an Jiaotong University, Xi'an 710049, People's Republic of China
Tel +86 298 265 5399
Email ruixiagao@mail.xjtu.edu.cn

Purpose: Androgen plays an important role in the progression of prostate cancer. In the present study, novel magnetic molecularly imprinted polymers (MMIPs) with good biocompatibility were produced for the selective separation and inhibition of testosterone in prostate cancer cells.

Materials and methods: MMIPs were prepared by using magnetic nanospheres, gelatin, and testosterone as the supporting materials, functional monomer, and the template molecule, respectively. The characterization of the resultant products was investigated by transmission electron microscopy, X-ray diffraction, and vibrating sample magnetometry. To test whether MMIPs can remove testosterone in biologic samples, human LNCaP (androgen-dependent) and C4-2 (androgen-independent) prostate cancer cells were selected as cell models. The translocation of androgen receptor (AR) was detected by immunofluorescence assay, and the expression of PSA mRNA was detected by real-time quantitative polymerase chain reaction analysis. Cell flow cytometry analysis was performed to detect cell cycle arrest.

Results: The synthesized nanomaterials (MMIPs) possessed high crystallinity, satisfactory superparamagnetic properties, and uniform imprinted shell, and exhibited high adsorption capacity, fast kinetics, and high selectivity for testosterone. Moreover, the obtained imprinted nanomaterials could selectively enrich and detect testosterone in the LNCaP cell samples as a solid-phase extractant coupled with high-performance liquid chromatography. In addition, the MMIPs could freely enter prostate cancer cells and suppress the translocation of AR into the cell nucleus. We further found that MMIPs inhibited upregulation of AR downstream target genes in LNCaP and C4-2 cells; also, MMIPs inhibited cell growth and induced obvious cell cycle arrest in androgen-dependent LNCaP cells, but had no obvious effect on androgen-independent C4-2 cells.

Conclusion: Our results indicate that the obtained imprinted nanomaterials can specifically and effectively bind testosterone and recover it from prostate cancer cells. Moreover, the MMIPs can freely enter prostate cancer cells and block the activation of testosterone-AR pathway. Thus, the MMIPs may be a new option for antiandrogen therapy in prostate cancer.

Keywords: magnetic separation, solid-phase extraction, testosterone, prostate cancer, androgen deprivation therapy, androgen receptor

Introduction

Testosterone (TSTO) is a naturally occurring androgenic steroid based on the cyclopentanoperhydrophenanthrene skeleton of four rings. TSTO is produced mainly in ovaries, testes, and adrenal cortex, which could maintain muscle strength and

bone density, and enhance physical fitness at proper levels.[1] Meanwhile, it is a vital indicator of pathologic conditions. Since androgens including TSTO promote the growth of prostate cancer, androgen deprivation therapy (ADT) is used as the first-line clinical approach at present to treat advanced prostate cancer, and it is also applied as adjuvant or neoadjuvant treatment for high-risk prostate cancer.[2] However, the suppression of endogenous TSTO production has deleterious effects on quality of life, including hot flushes, reduced mood and cognition, and weakened sexual function.[3,4] Therefore, it is meaningful to develop a method to specifically inhibit TSTO in prostate.

Molecularly imprinted polymers (MIPs), regarded as artificial antibodies, possess specific three-dimensional recognition cavities complementary to template in shape, size, and functionality. Their good physical and chemical stability, simple and economical production, durability, reusability, and high selectivity promote them to be widely applied in the fields of solid-phase extraction (SPE),[5,6] chemical and biochemical sensors,[7,8] heavy metals removal,[9] and drug delivery.[10] However, when traditional MIPs were used in the process of SPE, the centrifugation and filtration procedures were complex and time consuming. To solve this problem, Fe_3O_4 magnetic nanospheres have been introduced into MIPs through surface imprinting technique, because of their attractive superior properties such as small size, high surface-to-volume ratio, and magnetic susceptibility.[11–13] The resultant MIPs not only have strong specific recognition ability, but also can be easily localized at a designated area in the presence of an external magnetic field. Thus, magnetic MIPs (MMIPs) could be an ideal nanomolecule to bind and remove TSTO from the prostate.

In the present study, a novel type of magnetic imprinted nanopolymers with good biocompatibility was developed adopting Fe_3O_4 magnetic nanospheres, gelatin, and TSTO as carriers, functional monomer, and template molecule, respectively. The obtained MMIPs have spherical shape with a uniform and thin shell, and superparamagnetic property. Meanwhile, the resultant polymers exhibit fast kinetics, high adsorption capacity, excellent selectivity, and satisfactory reusability. The applicability of obtained MMIPs was investigated in the separation and determination of trace TSTO in LNCaP prostate cancer cell lysis solution. Moreover, it was determined whether the MMIPs suppress the function of TSTO in prostate cancer cells. We found that MMIPs could remove TSTO from prostate cancer cells and it may be a new option for the antiandrogen therapy in prostate cancer.

Materials and methods

Materials and apparatus

TSTO, dimethyl sulfoxide, methyltestosterone (MTSTO), testosterone propionate (TSTOP), 3-(4,5-dimethyl-2-thiazolyl)-2,5-diphenyl-2H-tetrazolium bromide (MTT), progesterone (PROG), and dihydrotestosterone (DHT) were purchased from Sigma-Aldrich (St Louis, MO, USA). Type-B gelatin and 3-aminopropyltriethoxysilane (APTES) were obtained from Alfa Aesar Chemical Company (Lancashire, UK). Ferric chloride hexahydrate ($FeCl_3 \cdot 6H_2O$), glutaraldehyde (GA), anhydrous sodium acetate (NaOAc), acetic acid (HAc), ethylene glycol, hydrochloric acid (HCl), ethanol, methanol, and trihydroxymethylaminomethane (Tris) were provided by Xi'an Chemicals Ltd (Xi'an, People's Republic of China). Enzalutamide (MDV3100) was purchased from Selleck Chemicals (Houston, TX, USA). All the reagents were reconstituted and stored following the protocol. Pure water (18.0 MΩ cm^{-1}) was produced by a WaterPro water system (TY10AXLC1805-2; Axlwater Corporation, Shanghai, People's Republic of China) and used throughout the experiment. LNCaP human prostate cancer cells were obtained from the American Type Culture Collection (Manassas, VA, USA). C4-2 cell line was a gift from Dr Jer-Tsong Hsieh of University of Texas Southwestern Medical Center[14,15] and the usage of this cell line was approved by the Institutional Review Board of the Medical School, Xi'an Jiaotong University. These two cell lines were cultured in Dulbecco's Modified Eagle's Medium/1640 supplemented with 10% fetal bovine serum (Thermo Fisher Scientific, Waltham, MA, USA) and 1% penicillin–streptomycin at 37°C in humidified air containing 5% CO_2. The morphology and structure of obtained materials were examined by a Tecnai G2 T2 S-TWIN transmission electron microscope. The infrared spectra were recorded on a Nicolet AVATAR-360 Fourier transform infrared spectrometer. The identification of the crystalline phase of resulted products was performed on a RigakuD/max/2500v/pc (Rigaku Corporation, Tokyo, Japan) X-ray diffractometer with a Cu Kα source. The 2θ angles probed were from 10° to 70° at a rate of 4° min^{-1}. The magnetic properties were analyzed with a vibrating sample magnetometer (LDJ 9600-1; LDJ Electronics, Troy, MI, USA). A Shimadzu high-performance liquid chromatography (HPLC) system equipped with LC-10AT pump, SPD-M 10A detector, CTO-10AS column oven, and Shimadzu VP-ODS C18 column (5 μm, 150×4.6 mm) was used. The column temperature was 30°C. The mobile phase was methanol–water (70:30, v/v) delivered at a flow rate of 1.0 mL min^{-1} and injection volume 20 μL, and the column effluent was monitored at 254 nm. The absorbance of LNCaP

cells was determined using a 96-well microplate reader (Bio-Rad Laboratories Inc., Hercules, CA, USA) at 490 nm.

Synthesis of Fe_3O_4@TSTO-MIPs

The monodispersed Fe_3O_4 nanospheres were prepared based on an earlier report.[16] The amino-modified Fe_3O_4 nanospheres (denoted as Fe_3O_4@NH_2) were prepared through sol–gel technique. Briefly, 0.2 g of Fe_3O_4 nanospheres was dissolved in a mixture of ethanol (100 mL) and highly purified water (20 mL) by stirring for 20 min, followed by the addition of HAc (2 mL) and APTES (0.6 mL). The mixture was made to react for 12 h at room temperature with continuous stirring. The obtained Fe_3O_4@NH_2 was collected with an external magnetic field and rinsed repeatedly with highly purified water and dried under vacuum. Then, the Fe_3O_4@NH_2 was modified sequentially with GA to introduce aldehyde groups. Two hundred milligrams of Fe_3O_4@NH_2 was dispersed in 20 mL of Tris-HCl buffer (10 mM, pH =7.0) and mixed with 0.65 mL of GA by sonication for 20 min. The mixture was then made to react at room temperature with continuous stirring for 6 h. The resulting aldehyde-functionalized Fe_3O_4 nanospheres (designed as Fe_3O_4@CHO) were collected by an external magnetic field and rinsed repeatedly with highly purified water and ethanol, and then dried under vacuum for further use.

The MMIPs of TSTO (designed as Fe_3O_4@TSTO-MIPs) were prepared as shown in Figure 1. Two hundred milligrams of gelatin was dissolved in 30 mL of Tris-HCl buffer (10 mM, pH =7.0) with stirring at 50°C for 1 h to allow the entire dissolution of gelatin. TSTO (30 mg) was dissolved in 10 mL of ethanol and mixed with the above solution. The mixture was stirred at 50°C for 2 h to form the TSTO–gelatin complex. Then, the Fe_3O_4@CHO (300 mg) was suspended into the above mixing solution and allowed to proceed for 9 h at 50°C. The resultant nanomaterials were rinsed with highly purified water and ethanol until the supernatant was clear. Next, 10 mL of ethanol–HAc (94:6, v/v) was added as an eluent at intervals of half an hour to remove the template molecule TSTO with the help of shaking until no adsorption was detected in the eluent by HPLC at about 254 nm to assure that the template was completely washed. The nanomaterials were collected by an external magnetic field and repeatedly washed with highly purified water and ethanol, then dried under vacuum, and the Fe_3O_4@TSTO-MIPs were obtained. For comparison,

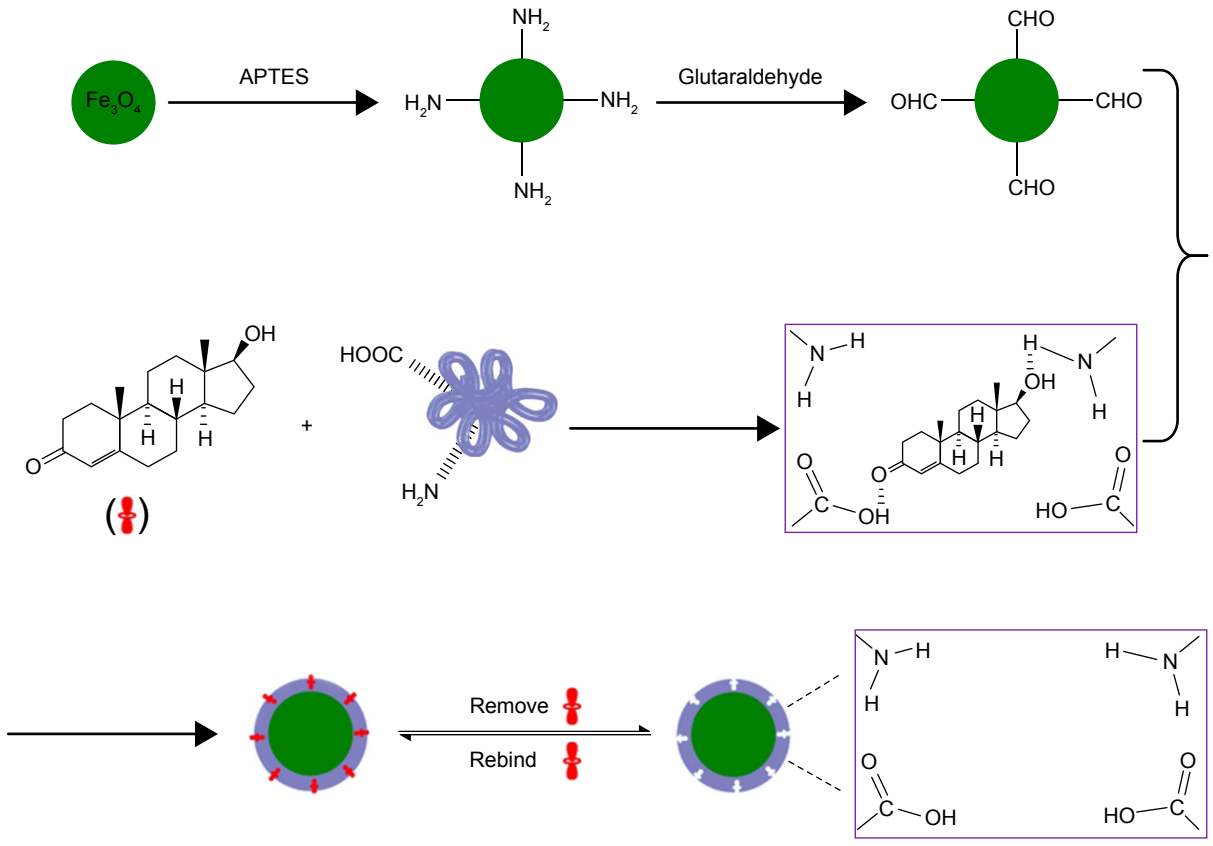

Figure 1 Schematic diagram of the synthetic route for Fe_3O_4@TSTO-MIPs.
Abbreviations: APTES, aminopropyltriethoxysilane; MIPs, molecularly imprinted polymers; TSTO, testosterone.

nonimprinted Fe_3O_4 nanospheres (designed as Fe_3O_4@NIPs) were prepared following the same procedures of Fe_3O_4@TSTO-MIPs in the absence of the template molecule TSTO.

Binding experiments of Fe_3O_4@TSTO-MIPs

To investigate the kinetics adsorption of the adsorbent, 10 mg of Fe_3O_4@TSTO-MIPs or Fe_3O_4@NIPs was added to 5 mL of ethanol with TSTO at a concentration of 24.0 μg mL^{-1} and incubated at regular time intervals from 5 to 60 min at room temperature. Then, the polymers were magnetically separated from the solution and the concentration of TSTO in the supernatant was measured by HPLC.

In the isothermal binding study, 10 mg of Fe_3O_4@TSTO-MIPs or Fe_3O_4@NIPs was added to 5 mL of ethanol solution with various initial concentrations (4.0–40 μg mL^{-1}) of TSTO. The mixture was shaken at room temperature for 35 min. Then, the polymers were magnetically isolated and the residual TSTO in the supernatant was determined by HPLC.

In the selectivity experiments, the mixed standard solution (5 mL) of TSTO, DHT, MTSTO, TSTOP, and PROG at an initial concentration of 24.0 μg mL^{-1} was incubated with 10 mg of Fe_3O_4@TSTO-MIPs or Fe_3O_4@NIPs at room temperature for 35 min; then, the extraction and detection procedures were conducted as described earlier in the kinetics adsorption experiments.

The adsorption capacity (Q) of the TSTO or competitive compounds bound to the imprinted polymers was determined using Equation 1:

$$Q = \frac{(C_0 - C_e)V}{W} \quad (1)$$

where C_0 and C_e (mg mL^{-1}) represent the initial and the equilibrium solution concentration of the adsorbed compounds, respectively, V (mL) represents the volume of the solution, and W (mg) is the weight of the imprinted polymers.

Additionally, the imprinting factor (IF) and the selectivity coefficient (SC) are used to evaluate the selectivity properties of Fe_3O_4@TSTO-MIPs. The IF and SC are calculated from the following equations:

$$IF = \frac{Q_{MIP}}{Q_{NIP}} \quad (2)$$

$$SC = \frac{IF_{TEM}}{IF_{COM}} \quad (3)$$

where Q_{MIP} and Q_{NIP} (mg g^{-1}) represent the adsorption capacity of Fe_3O_4@TSTO-MIPs and Fe_3O_4@NIPs, respectively, and IF_{TEM} and IF_{COM} are the IFs of template and competitive compounds, respectively.

Reusability of Fe_3O_4@TSTO-MIPs and Fe_3O_4@NIPs

To estimate the reusability of Fe_3O_4@TSTO-MIPs and Fe_3O_4@NIPs, 10 mg of nanomaterials was added to 10 mL of ethanol solution containing TSTO at a concentration of 24.0 μg mL^{-1}. The mixture was incubated at room temperature for 35 min. Then, the nanomaterials were collected by a magnet and the adsorption capacity for TSTO was detected by HPLC. The collected Fe_3O_4@TSTO-MIPs were washed with ethanol–HAc (94:6, v/v) for 6 h to ensure complete elution of residual TSTO and then washed with highly purified water for several times and dried under vacuum for reusing in successive adsorption of TSTO.

Determination of TSTO in human prostate cancer LNCaP cell sample

Fifty milliliters of LNCaP cells was spiked with TSTO at concentrations of 1.0, 5.0, and 50.0 ng mL^{-1}, respectively. Fifty milligrams of Fe_3O_4@TSTO-MIPs was added to the spiked cell sample and incubated at room temperature for 35 min. Next, the polymers were magnetically isolated, and Fe_3O_4@TSTO-MIPs which absorbed target molecules were eluted with a mixture of ethanol–HAc (94:6, v/v) solution. Then, the elution was collected and evaporated to dry under a stream of nitrogen and dissolved with 0.5 mL of methanol and measured by HPLC.

Real-time quantitative polymerase chain reaction assay

Cells were harvested with Trizol reagent (Thermo Fisher Scientific, Waltham, MA, USA) to extract total RNA and the procedures were described previously.[17] The primer sequences were as follows: PSA (F: 5′-GTGTGTGGACCTCCAT-GTTATT-3′, R: 5′-CCACTCACCTTTCCCCTCAAG-3′); FKBP5 (F: 5′-AATGGTG-AGGAAACGCCGATG-3′, R: 5′-TCGAGGGAATTTTAGGGAGACT-3′); TMPRSS2 (F: 5′-GTCCCCACTGTCTACGAGGT-3′, R: 5′-CAGACGACGGGGTTGGAAG-3′); and GAPDH (F: 5′-ATGGGGAAGGTGAAGGTCGG-3′, R: 5′-GACGGTGCCATGGA-ATTTGC-3′).

Immunofluorescence assay

Cells were cultured in a Millicell EZ SLIDE eight-well glass and washed with phosphate-buffered saline (PBS) three times

prior to being fixed in 4% paraformaldehyde for 30 min. Cells were subsequently washed with PBS again, treated with permeabilization solution (1% Triton X-100 in PBS), washed with PBS three times, and blocked with 1% bovine serum albumin (Sigma-Aldrich) in PBS for 1 h. Samples were subsequently incubated with anti-androgen receptor (AR) primary antibody (N-20; Santa Cruz Biotechnology Inc., Dallas, TX, USA) in antibody dilution buffer (1% bovine serum albumin in 1× PBS) overnight at 4°C. Samples were washed with PBS three times and incubated with secondary antibody fluorescein isothiocyanate-conjugated affinipure goat anti-rabbit IgG (#ZF-0315; dilution, 1:200; Beijing Zhongshan Golden Bridge Biotechnology, Co., Ltd.) for 60 min at room temperature, followed by DAPI staining (1:5,000) for 5 min in the dark. Samples were examined using laser scanning confocal microscopy (Nikon A1R/A1).

MTT assay

Cell viability and growth rate were measured by the MTT assay, as described previously.[18]

Flow cytometric analysis

Flow cytometric analysis was performed to evaluate the effects of MMIPs on cell cycle distribution, as we described previously.[19] Flow cytometry was performed using an FACS Calibur (Becton Dickinson, San Jose, CA, USA) system with CELLQuest software (version 3.3; Becton Dickinson). All experiments were carried out in triplicate to assess the consistency of response.

Statistical analysis

All the statistical analyses were performed with GraphPad Prism software (version 5.0), and Student's *t*-test was used for comparison of two groups. For each result, at least three independent experiments were performed to obtain statistical significance. $P<0.05$ was considered as statistically significant.

Results

Preparation of Fe_3O_4@TSTO-MIPs

The method for synthesis of Fe_3O_4@TSTO-MIPs through a multistep procedure is shown in Figure 1. Firstly, the Fe_3O_4 nanospheres were prepared by a modified solvothermal reaction.[16] Secondly, the Fe_3O_4 nanospheres were functionalized with APTES by a sol–gel process to obtain amine-modified Fe_3O_4 nanospheres (denoted as Fe_3O_4@NH_2).[20] Then, aldehyde-modified Fe_3O_4 nanospheres (denoted as Fe_3O_4@CHO) were obtained through imine bond formation between the aldehyde groups of GA and the amine groups of Fe_3O_4@NH_2. Next, the polymeric network was formed on the surface of Fe_3O_4@CHO by forming imine bonds between the aldehyde groups of Fe_3O_4@CHO and the amine groups of the template–monomer complex of TSTO and gelatin. Finally, after the removal of the template TSTO with ethanol-HAc (94:6, v/v) solution, Fe_3O_4@TSTO-MIPs with recognition cavities complementary to the template TSTO in shape, size, and functional group orientation were obtained.

Gelatin is a nontoxic, nonimmunogenic, and biodegradable biomacromolecule, which contains abundant active groups including NH_2, –COOH, and −OH and possesses native hydrophilic and hydrophobic segments.[21,22] These distinctive features make gelatin an ideal functional monomer agent to develop MIPs with good biocompatibility.

To obtain the best recognition performance of Fe_3O_4@TSTO-MIPs, the amount of gelatin ranging from 50 to 300 mg was evaluated. As shown in Figure 2, the amount of functional monomer affected the adsorption capacity greatly due to change in the number of recognition sites in the network of polymers. It was observed that *Q* and *IF* increased with an increase in the amount of gelatin from 50 to 200 mg, suggesting augmentation in the number of recognition cavities in the Fe_3O_4@TSTO-MIPs. However, the downtrends of *Q* and *IF* emerged with further increase in the mass of gelatin from 200 to 300 mg, which may be because excessive amount of functional monomer might lead to homogeneous self-condensation and decrease the number of recognition cavities. Herein, 200 mg of gelatin was adopted in our work.

Characterization of obtained nanomaterials

Figure 3 shows the transmission electron microscopy images of Fe_3O_4 and Fe_3O_4@TSTO-MIPs. Fe_3O_4 was obtained as

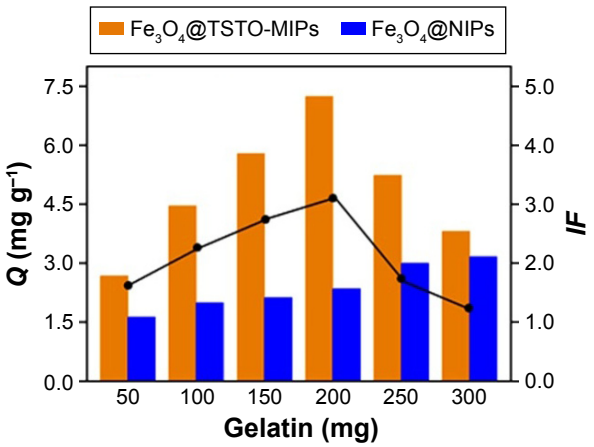

Figure 2 Effect of the amount of gelation on the imprinting performance of Fe_3O_4@TSTO-MIPs and Fe_3O_4@NIPs.
Abbreviations: *IF*, imprinting factor; MIPs, molecularly imprinted polymers; NIPs, nonimprinted polymers; TSTO, testosterone.

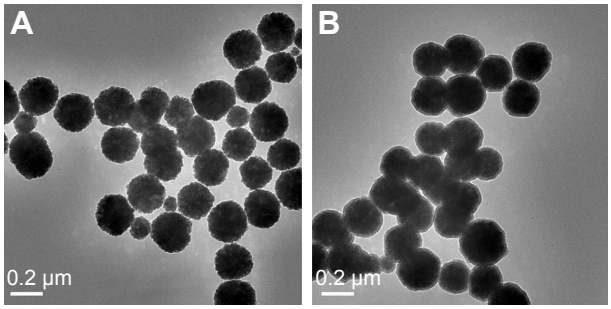

Figure 3 TEM images of Fe_3O_4 (**A**) and Fe_3O_4@TSTO-MIPs (**B**).
Abbreviations: MIPs, molecularly imprinted polymers; TEM, transmission electron microscopy; TSTO, testosterone.

spherical particles with an average size of about 200 nm (Figure 3A). After the coating process, an interface could be clearly distinguished between the inner Fe_3O_4 core and the outer imprinting shell, indicating that the preparation was successful. Meanwhile, the diameter of Fe_3O_4@TSTO-MIPs increased to around 220 nm (Figure 3B), corresponding to a 10 nm thickness of the imprinted shell, which would be beneficial for the mass transport between the solution and the surface of Fe_3O_4@TSTO-MIPs.

Fourier transform infrared spectra of Fe_3O_4, Fe_3O_4@NH_2, Fe_3O_4@CHO, and Fe_3O_4@TSTO-MIPs are shown in Figure 4A. The characteristic peaks of Fe–O group for all four samples were observed at around 586 cm^{-1}. Two peaks at 3,440 and 1,650 cm^{-1} (Figure 4A-c) assigned to stretching and bending vibrations of N–H indicate that the amino groups were modified on the magnetic nanospheres through a sol–gel technique. The peak at 1,722 cm^{-1} ascribed to the stretching vibration of carbonyl, and two typical peaks at 2,760 and 2,870 cm^{-1} attributed to the Fermi resonance frequency of vibrations of C–H exhibited that aldehyde groups were grafted to the Fe_3O_4@NH_2 (Figure 4A-d). For Fe_3O_4@TSTO-MIPs, the new peaks at 1,670 and 1,532 cm^{-1} corresponding to amide I (C=O stretching vibration) and amide II (N–H bending vibration) emerged (Figure 4A-b), implying that the imprinted shells have been coated onto the surface of Fe_3O_4.

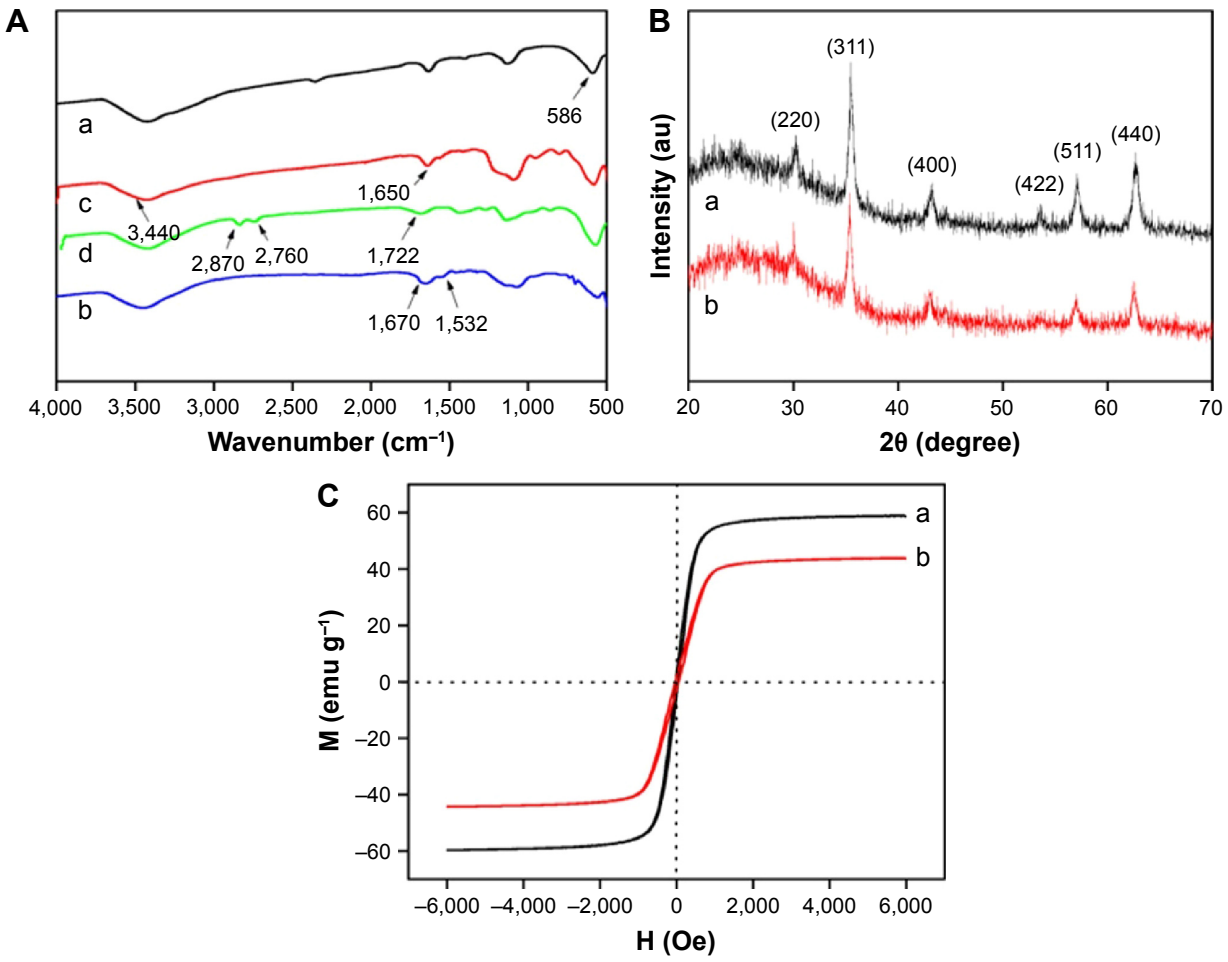

Figure 4 FT-IR spectra (**A**), XRD (**B**), and VSM (**C**) of Fe_3O_4 (a), Fe_3O_4@TSTO-MIPs (b), Fe_3O_4@NH_2 (c), and Fe_3O_4@CHO (d).
Abbreviations: FT-IR, Fourier transform infrared; MIPs, molecularly imprinted polymers; TSTO, testosterone; VSM, vibrating sample magnetometry; XRD, X-ray diffraction.

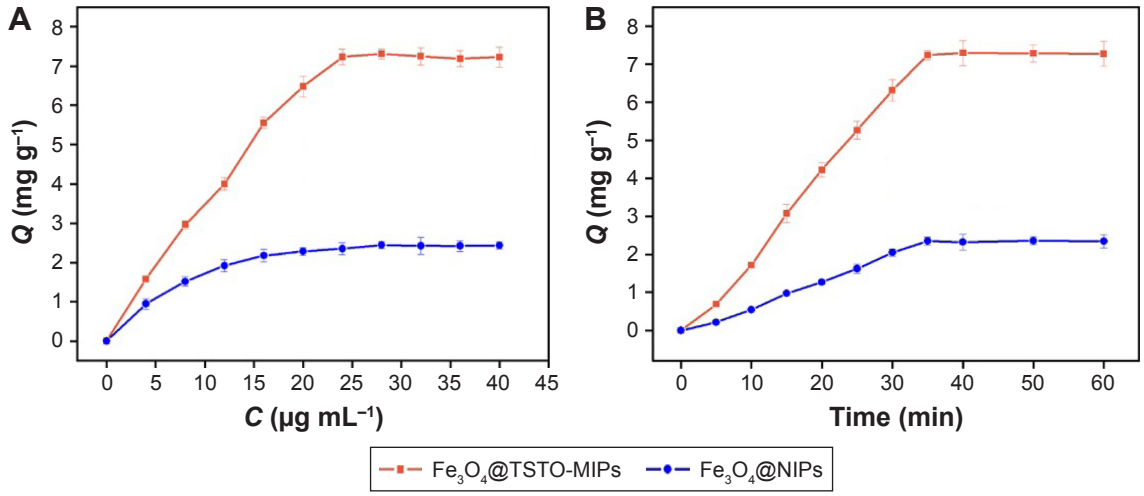

Figure 5 Adsorption isotherms (**A**) and kinetics (**B**) of Fe_3O_4@TSTO-MIPs and Fe_3O_4@NIPs toward TSTO.
Abbreviations: MIPs, molecularly imprinted polymers; NIPs, nonimprinted polymers; TSTO, testosterone.

Figure 4B illustrates the X-ray diffraction patterns of the synthesized Fe_3O_4 and Fe_3O_4@TSTO-MIPs. In the 2θ range of 20°–70°, six relatively discernible strong diffraction peaks for Fe_3O_4 (2θ =30.2°, 35.6°, 43.2°, 53.5°, 57.2°, and 62.8°) were observed for both samples. The peak positions at the corresponding 2θ values were indexed as (220), (311), (400), (422), (511), and (440), respectively, which were consistent with the database of magnetite in The Joint Committee on Powder Diffraction Standards (JCPDS)-International Center for Diffraction Data (JCPDS Card: 19–629) file. These results suggest that the crystalline nature of Fe_3O_4 core in the resultant polymers remained unchanged.

Figure 4C displays the magnetic hysteresis loops of Fe_3O_4 and Fe_3O_4@TSTO-MIPs at room temperature. It was obvious that both remanence and coercivity were ~0, suggesting that the samples were superparamagnetic. The saturation magnetization values were 58.79 and 43.82 emu g^{-1} for Fe_3O_4 and Fe_3O_4@TSTO-MIPs, respectively. The small decrease in saturation magnetization value demonstrated that the imprinted shell was thin, which could be effective to absorb and desorb template molecules between the solution and Fe_3O_4@TSTO-MIPs.

Binding properties of Fe_3O_4@TSTO-MIPs

The binding isotherms of TSTO onto Fe_3O_4@TSTO-MIPs and Fe_3O_4@NIPs are shown in Figure 5A. The adsorption capacity of TSTO bound to Fe_3O_4@TSTO-MIPs increased rapidly with an increase in initial concentration of TSTO, and then reached saturation when the initial concentration was above 24.0 μg mL^{-1}. Meanwhile, the amount of TSTO bound to Fe_3O_4@TSTO-MIPs at equilibrium concentration was dramatically higher than that of Fe_3O_4@NIPs, indicating that the imprinted cavities on the surface of Fe_3O_4@TSTO-MIPs were complementary to the template TSTO in shape, size, and functional groups.

The adsorption kinetic curves of TSTO absorbed on Fe_3O_4@TSTO-MIPs are shown in Figure 5B. It could be seen that the adsorption process was time dependent. The adsorption capacity increased rapidly in the first 25 min, and then the adsorption rate exhibited a slower increase to reach the adsorption equilibrium after 35 min. It is worth noting that the adsorption capacity of Fe_3O_4@TSTO-MIPs was much higher than that of Fe_3O_4@NIPs, suggesting the excellent imprinting effect of the imprinted polymers. These results manifested that the formed thin imprinted shell dramatically improved the mass transfer for easy diffusion of TSTO into the binding cavities.

Selectivity of Fe_3O_4@TSTO-MIPs

To investigate the selectivity of Fe_3O_4@TSTO-MIPs, four structural analogs (DHT, PROG, MTSTO, and TSTOP) were

Table 1 The adsorption capacity, imprinting factor, and selectivity coefficient of TSTO, DHT, MTSTO, PROG, and TSTOP for Fe_3O_4@TSTO-MIPs and Fe_3O_4@NIPs[a]

Targets	Q_{MIP} (mg g^{-1})	Q_{NIP} (mg g^{-1})	*IF*	*SC*
TSTO	5.24	1.51	3.47	–
DHT	3.61	1.43	2.52	1.38
MTSTO	2.96	1.34	2.21	1.57
PROG	2.11	1.49	1.42	2.44
TSTOP	1.43	1.37	1.04	3.34

Notes: [a]In this experiment, 10 mg of Fe_3O_4@TSTO-MIPs and Fe_3O_4@NIPs was incubated in the mixture of TSTO, DHT, PROG, MTSTO, and TSTOP with a concentration of 24 μg mL^{-1} in 5 mL of ethanol at room temperature for 35 min. n=5.
Abbreviations: DHT, dihydrotestosterone; *IF*, imprinting factor; MIPs, molecularly imprinted polymers; MTSTO, methyltestosterone; NIPs, nonimprinted polymers; PROG, progesterone; *SC*, selectivity coefficient; TSTO, testosterone; TSTOP, testosterone propionate.

selected as competitive compounds. As shown in Table 1, the Q of Fe_3O_4@TSTO-MIPs toward TSTO was higher than that of the other four analogs, suggesting that the imprinted nanomaterials had higher affinity for the template molecule than its analogs. Moreover, the recognition capacity of Fe_3O_4@TSTO-MIPs for the four analogs showed an appreciable difference with the order DHT>MTSTO>PROG>TSTOP. This may be because of their different molecular structures (Figure S1). They had a similar skeleton with the template molecule TSTO, except that DHT and MTSTO had an additional hydrogen atom and an extra methyl group, while the hydroxyl group of TSTO was replaced by the ketone group of PROG or the propionic group of TSTOP. The absence of hydroxyl group on PROG and TSTOP may account for their weaker ability to form hydrogen bond with gelatin, compared with DHT and MTSTO. Meanwhile, MTSTO and TSTOP possessed much more steric hindrance effect compared with TSTO and PROG, when recognized by Fe_3O_4@TSTO-MIPs. These results further demonstrated the satisfactory selectivity of Fe_3O_4@TSTO-MIPs.

Reusability of Fe_3O_4@TSTO-MIPs

The adsorption–desorption cycle was repeated six times by using the same Fe_3O_4@TSTO-MIPs to evaluate their stability, and the results are shown in Figure S2. The adsorption capacity of Fe_3O_4@TSTO-MIPs maintained at an almost steady value of 93.7% after six adsorption–regeneration cycles. The 6.3% decrease may be because some recognition cavities in the imprinted shells were clogged after regeneration or were destroyed after washing. The Q of Fe_3O_4@NIPs remained almost unchanged due to the nonspecific effect, thus the influence of washing procedures could be negligible. These results confirmed that Fe_3O_4@TSTO-MIPs are stable and have great potential for practical application.

Method validation and real sample analysis

The analytical performance of the methods, including linear range, limit of detection (LOD), precision, and accuracy, was investigated. A high correlation coefficient (0.9994) was obtained for TSTO in the linear concentration range of 1.0–100 ng mL^{-1}. LOD (signal to noise ratio=3) reflecting the sensitivity of the analytical method was found to be 0.05 ng mL^{-1}. The precision of the method was assessed by determining the relative standard deviations (RSDs) of intraday and interday at three different spiked levels. The results show that the RSD of intraday precision was 2.1%–3.2%, while that of interday precision was 3.7%–6.8%. To investigate the accuracy of the developed method, human prostate cancer LNCaP cell sample spiked with three levels (1.0, 5.0, and 50.0 ng mL^{-1}) of TSTO was analyzed. The recovery of TSTO ranged from 99.1% to 102.9% with RSD <6.8%, suggesting that the accuracy of Fe_3O_4@TSTO-MIPs coupled with HPLC was satisfactory for the analysis of trace TSTO in the human prostate cancer LNCaP cell samples.

Different strategies for determination of TSTO are listed briefly in Table 2. As can be seen, the present method had a relatively low LOD among the other reported approaches.[9,10,23,24] Meanwhile, Fe_3O_4@TSTO-MIPs used as SPE extractant possessed satisfactory selectivity and excellent stability, compared with the standard SPE C18 sorbents[24] and immunoaffinity capillary column,[10] respectively. In conclusion, the present method is reliable, effective, and sensitive.

The proposed method was applied for specific enrichment and determination of TSTO in the human prostate cancer LNCaP cell sample. The typical chromatograms of LNCaP cell sample spiked with TSTO at a concentration of 5.0 ng mL^{-1} and the elution of adsorbed Fe_3O_4@TSTO-MIPs are shown in Figure 6. Figure 6 shows that the peak of TSTO cannot be found from the chromatogram of the spiked LNCaP cell sample and there are some other peaks reflecting the LNCaP cell sample. After the enrichment of spiked LNCaP cell sample with Fe_3O_4@TSTO-MIPs and elution by ethanol–HAc (94:6, v/v) solution, the peak of TSTO was found distinctly at 5.40 min (Figure 6) and other interference peaks almost disappeared. The results verified that TSTO in spiked LNCaP cell sample could be selectively enriched

Table 2 Comparison with other published methods for the determination of TSTO

Analyte	Extractant	Analytical system	LOD	References
TSTO	MISPE	HPLC-DAD	0.47 ng mL^{-1}	23
TSTO	MISPE	LC–MS–MS	0.30 ng mL^{-1}	9
TSTO	SPE C18 sorbents	HPLC–MS–MS	2.0 ng L^{-1}	24
TSTO	Immunoaffinity capillary column	LIF	20 ng mL^{-1}	10
TSTO	Fe_3O_4@TSTO-MIPs	HPLC-UV	0.05 ng mL^{-1}	This study

Abbreviations: HPLC-DAD, high-performance liquid chromatography system equipped with a diode array detector; LC, liquid chromatography; LIF, laser-induced fluorescence detection; LOD, limit of detection; MIPs, molecularly imprinted polymers; MISPE, molecularly imprinted solid-phase extraction; MS, mass spectrometry; SPE, solid-phase extraction; TSTO, testosterone; UV, ultraviolet.

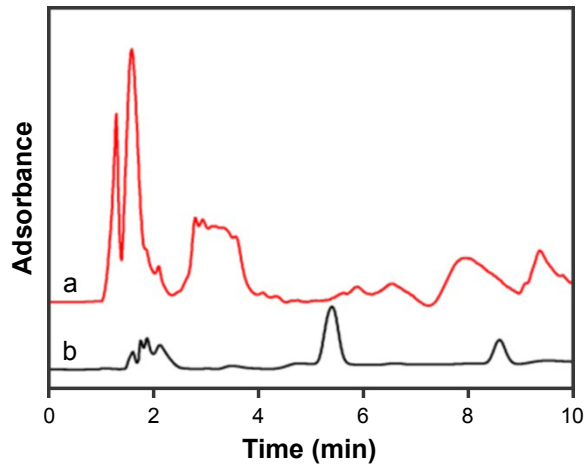

Figure 6 Chromatograms of the human prostate cancer LNCaP cell spiked with TSTO at the concentration of 5.0 ng mL^{-1} (a) and elution of absorbed Fe_3O_4@TSTO-MIPs (b).
Abbreviations: MIPs, molecularly imprinted polymers; TSTO, testosterone.

by Fe_3O_4@TSTO-MIPs and recovered by the washing step. Therefore, the developed method adopting Fe_3O_4@TSTO-MIPs as a solid-phase extractant coupled with HPLC in this study has favorable selectivity and anti-interference ability in real sample analysis.

MMIPs (Fe_3O_4@TSTO-MIPs) can freely enter prostate cancer cells

MMIPs (Fe_3O_4@TSTO-MIPs) were added into cell culture medium of LNCaP prostate cancer cells at 80, 160, and 320 μg mL^{-1} for 1 and 24 h, respectively, and then the cells were observed under a microscope. As shown in Figure 7, we found that MIP magnetic nanospheres could freely enter the cells and the state of cells was not changed within 24 h.

MMIPs inhibit the function of TSTO in prostate cancer cells

Since MMIPs can freely enter prostate cancer cells and TSTO should be absorbed by MMIPs, we further determined whether MMIPs could inhibit the function of TSTO in prostate cancer cells. AR is a type I nuclear receptor that can be activated by androgens such as TSTO and DHT, and the binding of androgen and AR triggers a cascade of events involving conformational changes and nuclear translocation, binding of AR dimer to the promoter and enhancer regions of target genes, and gene transcription.[25] Therefore, firstly, we found whether the treatment of MMIPs (160 μg mL^{-1}, 24 h) inhibited the nuclear translocation of AR in LNCaP and C4-2 prostate cancer cells by immunofluorescence assays, and castration medium without androgen and MDV3100 (20 nM, 24 h), which is a direct inhibitor of AR, were used as positive controls. We found that the nuclear translocation of AR in both LNCaP and C4-2 cells was dramatically inhibited by the treatment of MMIPs in cell culture medium (Figure 8). To detect whether the function of TSTO-AR was inhibited by MMIPs in prostate cancer cells, we treated LNCaP cells

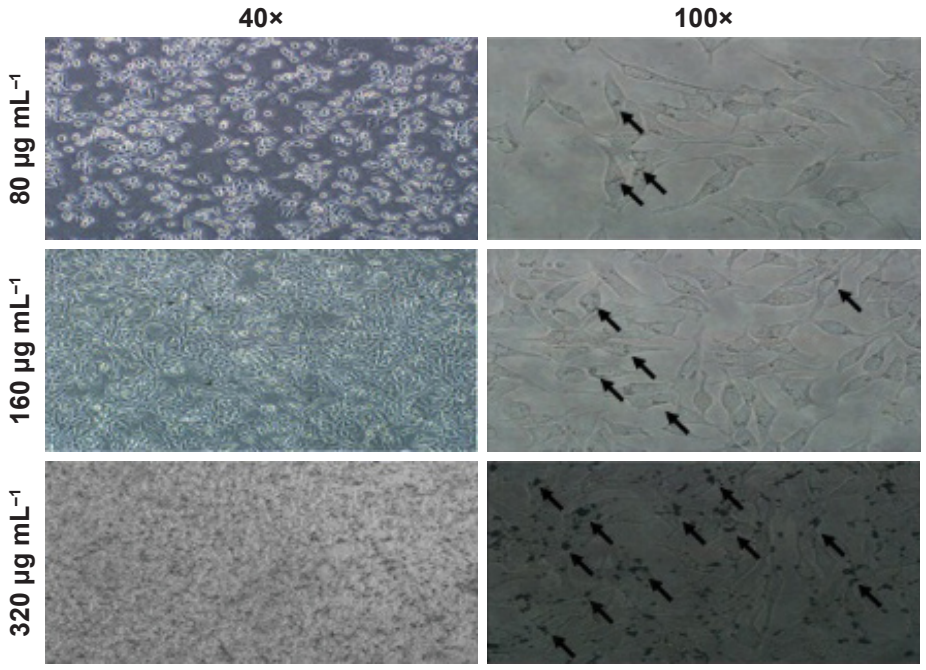

Figure 7 The state of prostate cancer cells after adding the MMIPs, observed under high-power microscope.
Notes: MMIPs could freely enter into the LNCaP prostate cancer cells with different concentrations of MMIPs after 24 h. Arrows indicate the locations of MMIPs inside cells.
Abbreviation: MMIPs, magnetic molecularly imprinted polymers.

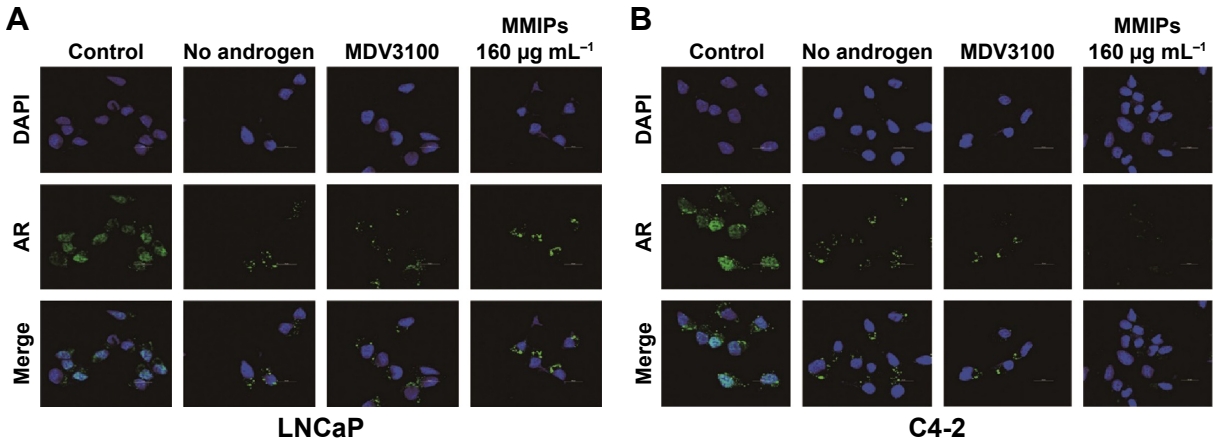

Figure 8 MMIPs inhibit the translocation of AR into nucleus of LNCaP (**A**) and C4-2 (**B**) prostate cancer cells, as detected by immunofluorescence assay.
Notes: AR was stained by fluorescein isothiocyanate (green). Control: normal cell culture medium. 40× magnification.
Abbreviations: AR, androgen receptor; MMIPs, magnetic molecularly imprinted polymers.

and C4-2 cells with regular medium (control), medium with charcoal-stripped serum (which does not contain androgen), 20 nM of MDV3100, 80 μg mL^{-1} of MMIPs, 160 μg mL^{-1} of MMIPs, and 320 μg mL^{-1} of MMIPs, respectively, and determined the expression of PSA, FKBP5, and TMPRSS2, which are the target genes of TSTO-AR, through real-time quantitative polymerase chain reaction assays. Moreover, to confirm whether MMIPs absorb TSTO specifically, we also treated those cells with 10 ng mL^{-1} of DHT in six other groups. We found that the expression levels of TSTO-AR target genes decreased when cells were treated with CSS, MDV3100, and MMIPs; on the other hand, DHT could rescue the suppression of AR target genes by MMIP treatment (Figure 9), suggesting that MMIPs inhibited the function of TSTO-AR, but not DHT-AR in prostate cancer cells, and the inhibition was through the binding of MMIPs with TSTO, but not DHT. Taken together, our results indicate that MMIPs can inhibit the activation of TSTO-AR pathway through binding with TSTO and sequestering AR in cell cytoplasm in prostate cancer cells.

MMIPs inhibited cell proliferation and induced cell cycle arrest in LNCaP, but not C4-2 prostate cancer cells

To further determine whether MMIPs suppress the effect of TSTO on prostate cancer cells, we treated androgen-dependent LNCaP prostate cancer cells and androgen-independent C4-2 cells, whose growth is promoted by oncogenic pathways other than androgen-triggering AR activity, with different concentrations of MMIPs and measured cell growth by MTT assays. As shown in Figure 10A, we found that MMIPs inhibited cell growth of LNCaP cells in a dose-dependent and time-dependent manner, indicating that MMIPs inhibited the effect of TSTO on prostate cancer cell growth. Furthermore, we detected whether MMIPs inhibited cell growth through the suppression of cell cycle progression by cell flow cytometry analysis, and found that MMIPs induced G1 cell cycle arrest in LNCaP cells (Figure 11A). On the other hand, MMIP treatment did not affect the cell growth and cell cycle progression of C4-2 cells (Figures 10B and 11B). Our results indicate that MMIPs can block the function of TSTO in cell growth and cell cycle progression of early-stage prostate cancer cells.

Discussion

Prostate cancer is one of the most common malignancies in males in the USA.[26] In the present study, to remove androgen from prostate cancer cells, novel MMIPs, Fe_3O_4@TSTO-MIPs, using TSTO as the template molecule, were synthesized and characterized. They possessed high crystallinity and satisfactory superparamagnetic properties, and the obtained polymers exhibited fast kinetics, high adsorption capacity, and excellent selectivity for the template molecule TSTO. Subsequently, we found that the imprinted nanomaterials could successfully recover TSTO in LNCaP prostate cancer cell samples and freely enter LNCaP cells. Furthermore, MMIPs could suppress the translocation of AR into cell nucleus, inhibit the function of AR, and induce obvious cell cycle arrest in LNCaP cells. Taken together, our results indicate that the new synthesized Fe_3O_4@TSTO-MIP is an efficient carrier to remove or recover TSTO from the cell lysates and living cells.

Application of ADT in prostate cancer is increasing in recent years.[2] ADT can be applied by orchiectomy (castration) in surgery or by taking a gonadotropin-releasing hormone agonist or a gonadotropin-releasing hormone

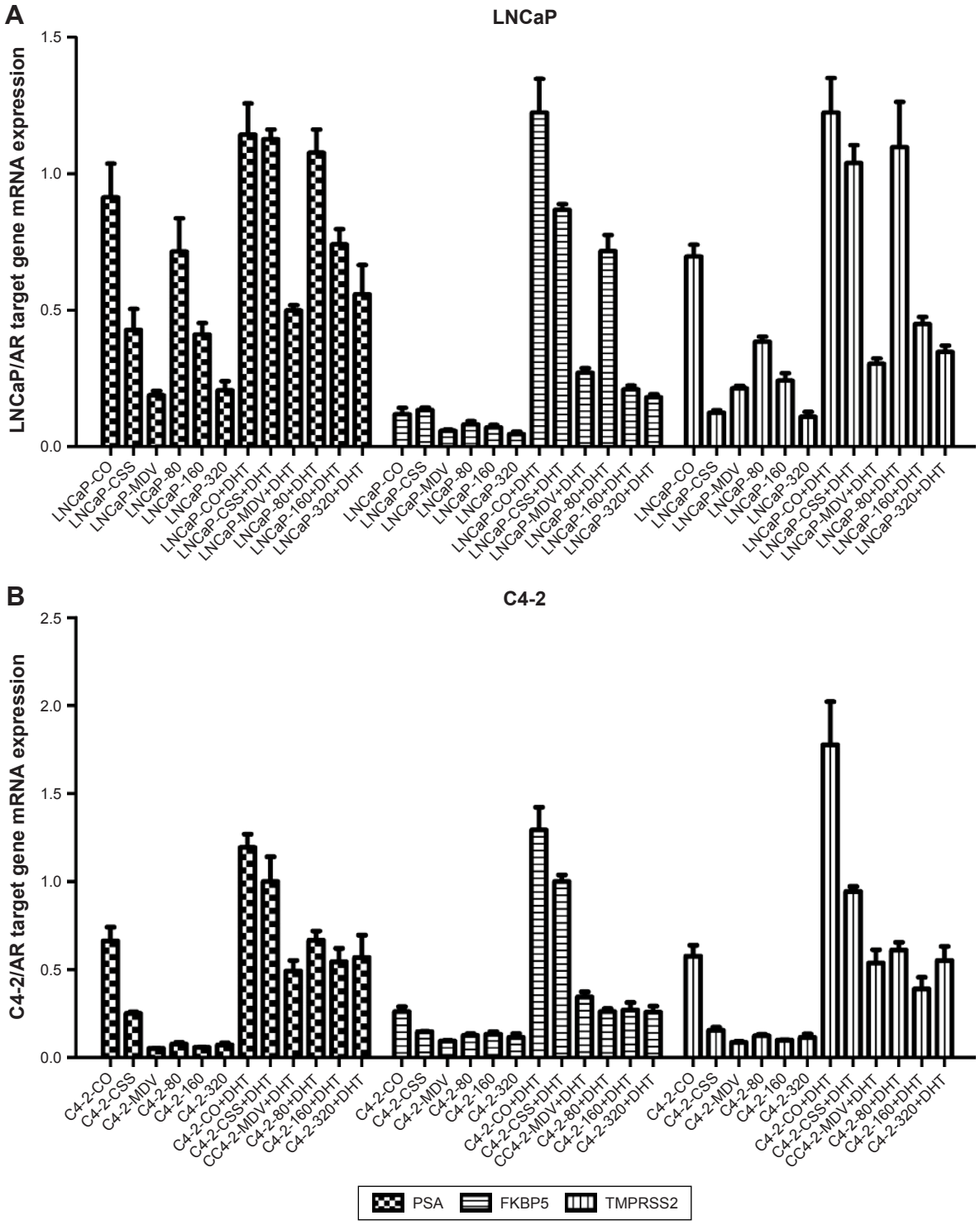

Figure 9 MMIPs inhibit the expression of AR downstream target genes in LNCaP (**A**) and C4-2 (**B**) prostate cancer cells, as detected by real-time quantitative polymerase chain reaction assay.

Notes: Cells were treated with normal cell culture medium (control), medium without androgen (no androgen), MDV3100, and different concentration of MMIPs for 24 h, and then 10 ng mL^{-1} DHT was added and made to react for 12 h.

Abbreviations: AR, androgen receptor; DHT, dihydrotestosterone; MMIPs, magnetic molecularly imprinted polymers.

antagonist orally. All these methods block TSTO in the whole body, leading to several side effects, such as adverse bone and cardiometabolic effects, in prostate cancer patients.[3,4] In this study, we found that Fe_3O_4@TSTO-MIPs could inhibit the translocation of AR into cell nucleus and the upregulation of AR downstream target genes, such as PSA and FKBP5, in LNCaP and C4-2 cells, indicating that Fe_3O_4@TSTO-MIPs block the androgen-AR pathway in prostate cancer

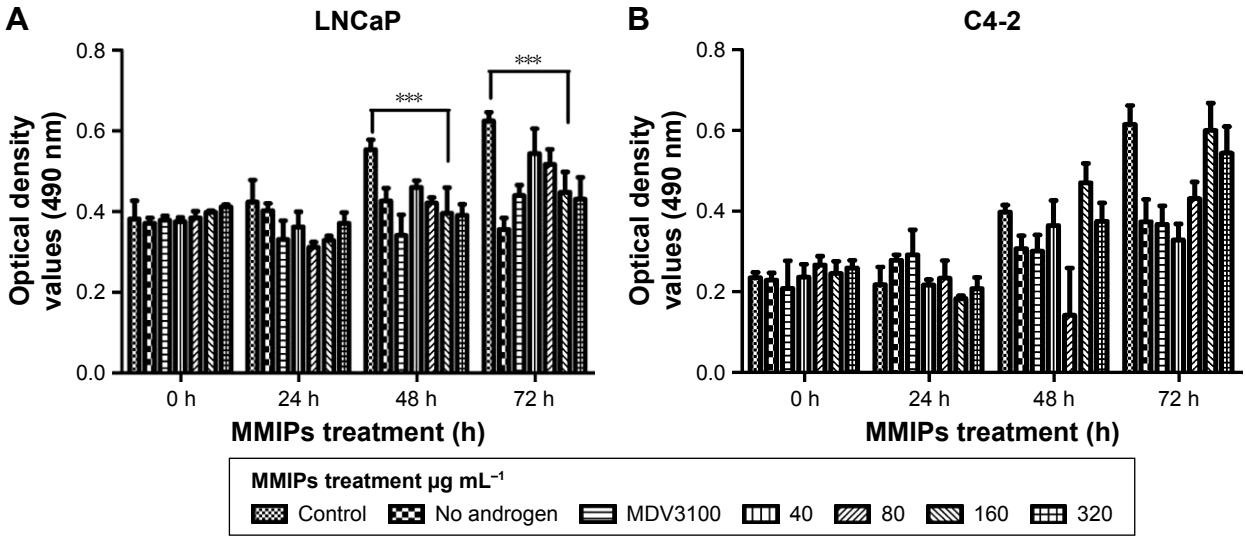

Figure 10 MMIPs inhibit cell growth of LNCaP cells (**A**), but not C4-2 cells (**B**), as detected by MTT assay.
Notes: Cells were treated with 160 μg mL^{-1} of MMIPs for 0, 24, 48, and 72 h, respectively. ***$P<0.001$.
Abbreviations: MMIPs, magnetic molecularly imprinted polymers; MTT, 3-(4,5-dimethyl-2-thiazolyl)-2,5-diphenyl-2H-tetrazolium bromide.

cells through binding to TSTO and sequestrating it in the cell cytoplasm. Interestingly, the induction of AR target genes blocked by Fe_3O_4@TSTO-MIPs can be restored by DHT, which is another kind of androgen, further confirming the binding specify of Fe_3O_4@TSTO-MIPs on TSTO. Moreover, the cell growth of androgen-sensitive LNCaP cells was inhibited by Fe_3O_4@TSTO-MIPs in a dose- and time-dependent manner, but they had no obvious effect on the growth of androgen-independent C4-2 cells, suggesting that Fe_3O_4@TSTO-MIPs inhibit cell growth specifically through inhibiting TSTO function, but do not have nonspecific effects. Notably, a part of AR in the C4-2 cells is mutated and can be activated by oncogenic pathways such as STAT3, which promotes cell proliferation without androgen stimulation. This is why, the growth of C4-2 cells is not dependent on androgen and Fe_3O_4@TSTO-MIPs cannot inhibit the proliferation of C4-2 cells. In summary, our data indicate that Fe_3O_4@TSTO-MIPs can specifically block TSTO function in prostate cancer cells and it may be a new option for the antiandrogen therapy in prostate cancer.

MIPs can recognize molecular targets with very high selectivity due to their specific binding sites with complementary size, shape, and functional groups to the template molecules.[27–29] Moreover, surface imprinting has adopted various supports such as Fe_3O_4 magnetic nanospheres during the past years,[16,30,31] which can efficiently separate complicated matrices with an external magnet. To date, TSTO-imprinted polymers that were previously reported have been mostly prepared in organic solvents,[11–13] which could lead to poor recognition ability in biologic samples. The Fe_3O_4@TSTO-MIPs we synthesized can not only recognize TSTO specifically with high affinity in human cells, which suggests that it can be used to determine the concentration of androgens in body liquid, different cells and organs, but also inhibit the function of TSTO through binding to it and sequestrating it in the cell cytoplasm. In addition, since it is a kind of magnetic nanosphere, it could be guided to a designated area in the body, such as prostate. Thus, its particular advantage in the ADT is that the inhibition on TSTO could be limited in the prostate and the function of TSTO in other organs will not be affected. The application of Fe_3O_4@TSTO-MIPs in the ADT of early-stage prostate cancer may block the function of TSTO and inhibit cell proliferation efficiently while causing lesser side effects.

Conclusion

A simple and mild approach was developed to prepare a novel kind of magnetic imprinted nanospheres with good biocompatibility for isolation and detection of TSTO in biologic samples. The obtained imprinted nanomaterials exhibited fast kinetics, high adsorption capacity, and satisfactory selectivity. The obtained imprinted nanomaterials used as solid-phase sorbents coupled with HPLC were successfully applied for the selective adsorption and determination of TSTO in the LNCaP cell samples. Moreover, MMIPs can freely enter LNCaP cells and inhibit the function of AR, and induce obvious cell cycle arrest in LNCaP cells by sequestrating AR in the cell cytoplasm. Taken together, our results indicate that

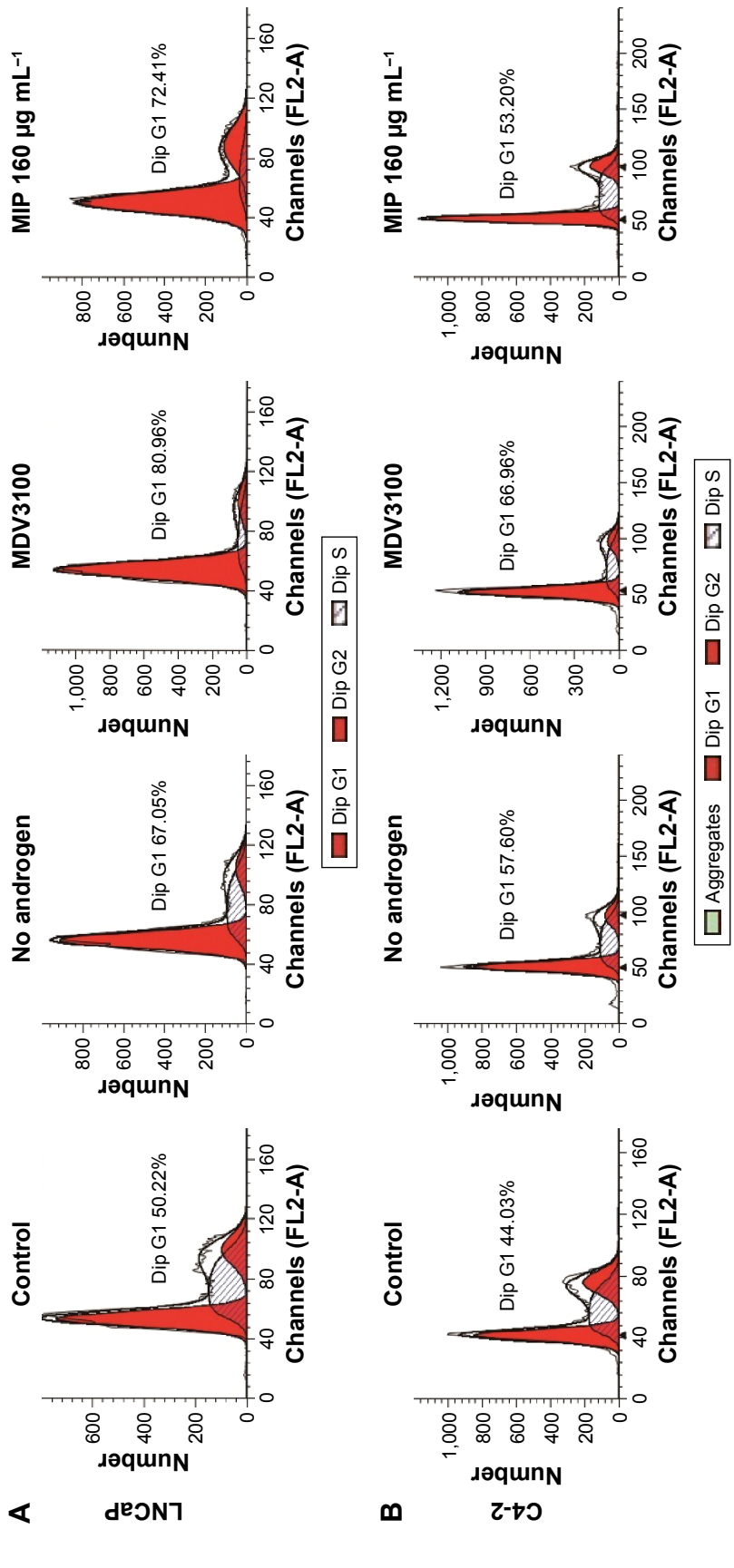

Figure 11 MMIPs induce cell cycle arrest in LNCaP cells (**A**), but not C4-2 cells (**B**), as detected by cell flow cytometric analysis.
Abbreviation: MMIPs, magnetic molecularly imprinted polymers.

the newly synthesized Fe_3O_4@TSTO-MIPs is an efficient carrier to remove or recover TSTO from the cell lysates and living cells, and it could be a new option for antiandrogen therapy in prostate cancer.

Acknowledgments

This work was supported by the National Natural Science Foundation of China grants (No 81372279 and 81672557 to P Guo), the Fundamental Research Funds for the Central Universities (No xjj2016101 to X Tang), and China Postdoctoral Science Foundation (No 2016M600800 to X Tang).

Disclosure

The authors report no conflicts of interest in this work.

References

1. Zitzmann M, Nieschlag E. Testosterone levels in healthy men and the relation to behavioural and physical characteristics: facts and constructs. *Eur J Endocrinol*. 2001;144(3):183–197.
2. Abrahamsson PA. Potential benefits of intermittent androgen suppression therapy in the treatment of prostate cancer: a systematic review of the literature. *Eur Urol*. 2010;57(1):49–59.
3. Allan CA, Collins VR, Frydenberg M, McLachlan RI, Matthiesson KL. Androgen deprivation therapy complications. *Endocr Relat Cancer*. 2014;21(4):T119–T129.
4. Ostergren PB, Kistorp C, Bennedbaek FN, Faber J, Sonksen J, Fode M. The use of exercise interventions to overcome adverse effects of androgen deprivation therapy. *Nat Rev Urol*. 2016;13(6):353–364.
5. Bagheri H, Molaei K, Asgharinezhad AA, Ebrahimzadeh H, Shamsipur M. Magnetic molecularly imprinted composite for the selective solid-phase extraction of p-aminosalicylic acid followed by high-performance liquid chromatography with ultraviolet detection. *J Sep Sci*. 2016;39(21): 4166–4174.
6. Gao R, Kong X, Wang X, He X, Chen L, Zhang Y. Preparation and characterization of uniformly sized molecularly imprinted polymers functionalized with core-shell magnetic nanoparticles for the recognition and enrichment of protein. *J Mater Chem*. 2011;21(44):17863–17871.
7. Cheng Z, Dai Y, Kang X, et al. Gelatin-encapsulated iron oxide nanoparticles for platinum (IV) prodrug delivery, enzyme-stimulated release and MRI. *Biomaterials*. 2014;35(24):6359–6368.
8. Bajpai AK, Choubey J. Design of gelatin nanoparticles as swelling controlled delivery system for chloroquine phosphate. *J Mater Sci Mater Med*. 2006;17(4):345–358.
9. Bui BTS, Merlier F, Haupt K. Toward the use of a molecularly imprinted polymer in doping analysis: selective preconcentration and analysis of testosterone and epitestosterone in human urine. *Anal Chem*. 2010;82(11):4420–4427.
10. Chen HX, Huang T, Zhang XX. Immunoaffinity extraction of testosterone by antibody immobilized monolithic capillary with on-line laser-induced fluorescence detection. *Talanta*. 2009;78(1):259–264.
11. He C, Long Y, Pan J, Li K, Liu F. Molecularly imprinted silica prepared with immiscible ionic liquid as solvent and porogen for selective recognition of testosterone. *Talanta*. 2008;74(5):1126–1131.
12. Tan Y, Jing L, Ding Y, Wei T. A novel double-layer molecularly imprinted polymer film based surface plasmon resonance for determination of testosterone in aqueous media. *Appl Surf Sci*. 2015;342: 84–91.
13. Augustine A, Mathew B. Synthesis of carbon nanotube incorporated molecular imprinted polymer with binding affinity towards testosterone. *ISRN Poly Sci*. 2014;2014:790583.
14. Wu HC, Hsieh JT, Gleave ME, Brown NM, Pathak S, Chung LW. Derivation of androgen-independent human LNCaP prostatic cancer cell sublines: role of bone stromal cells. *Int J cancer*. 1994;57(3):406–412.
15. Thalmann GN, Anezinis PE, Chang SM, et al. Androgen-independent cancer progression and bone metastasis in the LNCaP model of human prostate cancer. *Cancer Res*. 1994;54(10):2577–2581.
16. Gao R, Mu X, Zhang J, Tang Y. Specific recognition of bovine serum albumin using superparamagnetic molecularly imprinted nanomaterials prepared by two-stage core-shell sol-gel polymerization. *J Mater Chem B*. 2014;2(7):783–792.
17. Jia J, Li F, Tang XS, et al. Long noncoding RNA DANCR promotes invasion of prostate cancer through epigenetically silencing expression of TIMP2/3. *Oncotarget*. 2016;7(25):37868–37881.
18. Gao Y, Shi Q, Xu S, et al. Curcumin promotes KLF5 proteasome degradation through downregulating YAP/TAZ in bladder cancer cells. *Int J Mol Sci*. 2014;15(9):15173–15187.
19. Li F, Zeng J, Gao Y, et al. G9a Inhibition induces autophagic cell death via AMPK/mTOR Pathway in Bladder Transitional Cell Carcinoma. *PLoS One*. 2015;10(9):e0138390.
20. Hao Y, Gao R, Shi L, Liu D, Tang Y, Guo Z. Water-compatible magnetic imprinted nanoparticles served as solid-phase extraction sorbents for selective determination of trace 17beta-estradiol in environmental water samples by liquid chromatography. *J Chromatogr A*. 2015;1396:7–16.
21. Huang S, Deng T, Wang Y, et al. Multifunctional implantable particles for skin tissue regeneration: preparation, characterization, in vitro and in vivo studies. *Acta Biomater*. 2008;4(4):1057–1066.
22. Rivadeneira J, Laura Di Virgilio A, Carina Audisio M, Boccaccini AR, Gorustovich AA. Evaluation of the antibacterial effects of vancomycin hydrochloride released from agar-gelatin-bioactive glass composites. *Biomed Mater*. 2015;10(1):015011.
23. Ricanyova J, Gadzala-Kopciuch R, Reiffova K, Bazel Y, Buszewski B. Molecularly imprinted adsorbents for preconcentration and isolation of progesterone and testosterone by solid phase extraction combined with HPLC. *Adsorpt J Int Adsorpt Soc*. 2010;16(4–5):473–483.
24. Danaceau JP, Morrison MS, Slawson MH. Quantitative confirmation of testosterone and epitestosterone in human urine by LC/Q-ToF mass spectrometry for doping control. *J Mass Spectrom*. 2008;43(7):993–1000.
25. Haile S, Sadar MD. Androgen receptor and its splice variants in prostate cancer. *Cell Mol Life Sci*. 2011;68(24):3971–3981.
26. Siegel RL, Miller KD, Jemal A. Cancer statistics, 2015. *CA Cancer J Clin*. 2015;65(1):5–29.
27. Chough SH, Park KH, Cho SJ, Park HR. In situ preparation of powder and the sorption behaviors of molecularly imprinted polymers through the complexation between polymer ion of methyl methacrylate/acrylic acid and Ca++ ion. *Anal Chim Acta*. 2014;841:84–90.
28. Han S, Li X, Wang Y, Chen S. Graphene oxide-based fluorescence molecularly imprinted composite for recognition and separation of 2,4,6-trichlorophenol. *RSC Adv*. 2015;5(3):2129–2136.
29. Wang X, Kang Q, Shen D, Zhang Z, Li J, Chen L. Novel monodisperse molecularly imprinted shell for estradiol based on surface imprinted hollow vinyl-SiO2 particles. *Talanta*. 2014;124:7–13.
30. Gao R, Hao Y, Zhao S, et al. Novel magnetic multi-template molecularly imprinted polymers for specific separation and determination of three endocrine disrupting compounds simultaneously in environmental water samples. *RSC Adv*. 2014;4(100):56798–56808.
31. Liang Y, He X, Chen L, Zhang Y. Preparation and characterization of TiO2-Graphene@Fe3O4 magnetic composite and its application in the removal of trace amounts of microcystin-LR. *RSC Adv*. 2014; 4(100):56883–56891.

Supplementary materials

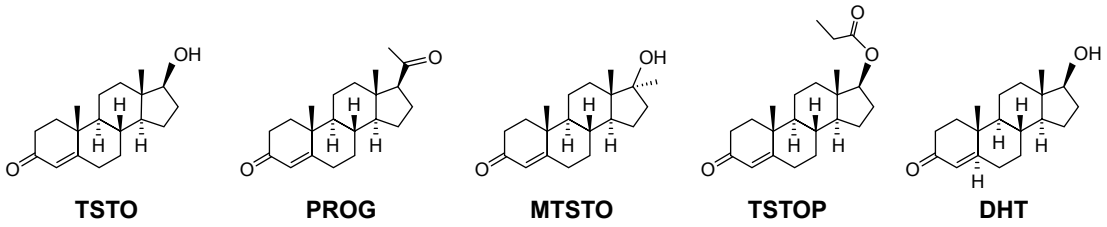

Figure S1 Molecular structures of template and other analogs.
Abbreviations: DHT, dihydrotestosterone; MTSTO, methyltestosterone; PROG, progesterone; TSTO, testosterone; TSTOP, testosterone propionate.

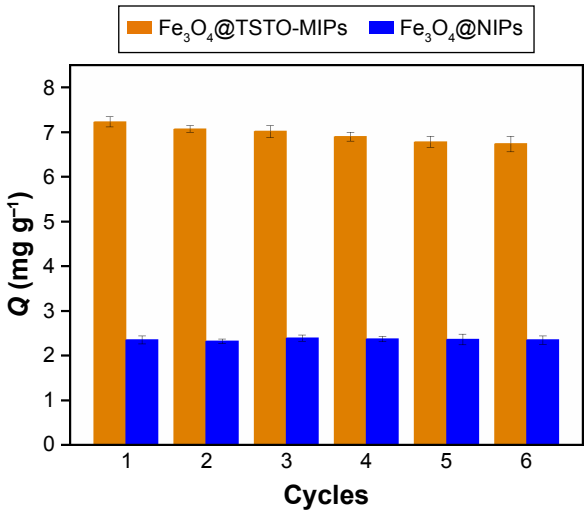

Figure S2 The reusability of Fe_3O_4@TSTO-MIPs and Fe_3O_4@NIPs toward TSTO.
Abbreviations: MIPs, molecularly imprinted polymers; NIPs, nonimprinted polymers; TSTO, testosterone.